

# TRAJECTORIES LEAVING A SPHERE IN THE RESTRICTED 3-BODY PROBLEM

**Carlo von Kirchbach\*, Huan Zheng\*,  
Jeffrey Aristoff\*, Jonathan Kavanagh\*,  
Benjamin Villac<sup>†</sup>, Martin Lo<sup>‡</sup>**

The set of trajectories leaving/impacting the surface of the Galilean satellites of Jupiter is analyzed from theoretical and computational viewpoints in the circular restricted three body problem in order to characterize the sensitive impact regions for spacecraft trajectory applications, as well as the main dynamical structures influencing this set of trajectories. A set of escape/impact dynamical maps as a function of the Jacobi constant has been computed and their analysis, using a two body approximation and the stable/unstable manifolds associated with the colinear libration point dynamics, is presented. While the results mainly focus on the planar problem, the two body analysis also considers the spatial problem.

## INTRODUCTION

The orbital dynamics around a Galilean moon of Jupiter, Europa, present many unstable regions due to the large gravitational perturbations coming from Jupiter, and can result in the impact of a spacecraft without control in a matters of days. This fact is of particular importance to designers of orbital transfers when robustness with respect to mis-thrust direction or loss of thrust during a transfer around one these moon is considered.

In order to analyze the impact/non-impact characteristics of some of these dynamics, the trajectories leaving the surface of Europa have been analyzed. This set of trajectories represents, indeed, a first approximation to the set of possible transfer trajectories that would result from a single impulsive maneuver of a Europa orbiter on a low altitude, nearly circular orbit. The study of such a set represents a first step toward the understanding of the larger space of possible transfers. While an investigation of these single impulse

---

\*University of California at Los Angeles (UCLA), Institute for Pure and Applied Mathematics (IPAM), Research in Industrial Problems for the Summer (RIPS), 2004, JPL team member.

<sup>†</sup>Staff member of the engineering staff, Jet Propulsion Laboratory, California Institute of Technology, 4800 Oak Grove Drive, Pasadena, CA 91109. E-mail: Benjamin.F.Villac@jpl.nasa.gov

<sup>‡</sup>Senior member of engineer staff, Jet Propulsion Laboratory, California Institute of Technology, 4800 Oak Grove Drive, Pasadena, CA 91109.

transfers over a single orbit was considered in references (Ref. 10) and (Ref. 11), no attempt was made to explore the set of impact trajectories over a longer time span, which represents the focus of this paper. To reach this goal, the set of trajectories leaving the surface of Europa has been numerically integrated over a fixed time span ( $\approx 100$  days) in the restricted three body problem\* in order to generate dynamical maps of the impact properties of these trajectories.

Friedlander<sup>2</sup> studied a similar problem in relation to the Pioneer and Mariner missions. His study focused, however, on the estimation of the likelihood of a Jupiter orbiter to impact with any of the different Galilean Moons for a restricted class of orbits and was not concerned with mapping the associated dynamics. On the contrary, this paper focuses on the dynamics that would influence an orbiter starting in the vicinity of one of the Galilean Moons, presents some global maps for these dynamics and attempts to extract some of the main dynamical phenomena influencing them.

After presenting the model and algorithms used, and the numerical maps obtained, two theoretical tools for characterizing some of the features observed on these maps are presented. For low energies, the invariant manifolds associated with the libration point dynamics<sup>1</sup> are computed and applied to the above maps. For higher energies, the two body approximation, obtained by neglecting the gravitational effect of Europa, is used to complement the insights obtained via the invariant manifold theory.

## DYNAMICS

This section briefly reviews the basic features of the dynamical model used in this study, the circular restricted three body problem (CR3BP), in order to introduce some of the numerical parameters and conventions used. More information on this model can be found, for example, in (Ref. 8) and (Ref. 9). While the method and some of the results presented in this paper are not restricted to the Europa-Jupiter system, the numerical constants are chosen to model such a system for its intrinsic interest for future space missions. The massive body (primary) will thus be referred to as Jupiter, while the secondary will be referred to as Europa.

### The Equations of Motion

The circular restricted three body problem is an approximation to the more complex three body problem, which captures the main dynamical features of the dynamics of planetary satellites<sup>†</sup> and has been extensively used in spacecraft trajectory design over the past decade<sup>5,3,4</sup>.

We recall that the CR3BP can be normalized by setting the distance between Europa

---

\*Emphasis has been placed on the planar problem, though the theoretical investigations using the two body dynamics have also been performed in the spatial problem.

<sup>†</sup>At least, when the time scale considered is not too long, as for example in the case of spacecraft transfers.

and Jupiter to one distance unit, the combined mass of the two celestial bodies to one mass unit and choosing the time unit so that the value of the universal constant of gravitation is one in these units. It is then convenient to introduce the parameters  $\mu$  and  $\nu = 1 - \mu$ , where:

$$\mu = \frac{M_m}{M_m + M_j}$$

since the normalized mass of Europa is then equal to  $\mu$ , the one of Jupiter to  $\nu$  and Jupiter and Europa are separated by a normalized distance of  $\mu$  and  $\nu$  from their common barycenter, respectively.

Defining a non-inertial frame of reference, centered at the barycenter of the Jupiter-Europa system, rotating with constant unit angular velocity,  $\omega$ , with respect to an inertial frame, and presenting its  $x$ -axis along the Jupiter-Europa line, its  $z$ -axis along  $\omega$ , and its  $y$ -axis to complete the right-handed orthogonal reference frame, Jupiter and Europa are then fixed on the  $x$ -axis of this frame at the coordinates  $-\mu$  and  $\nu$ , respectively. This situation is illustrated in Figure 1.

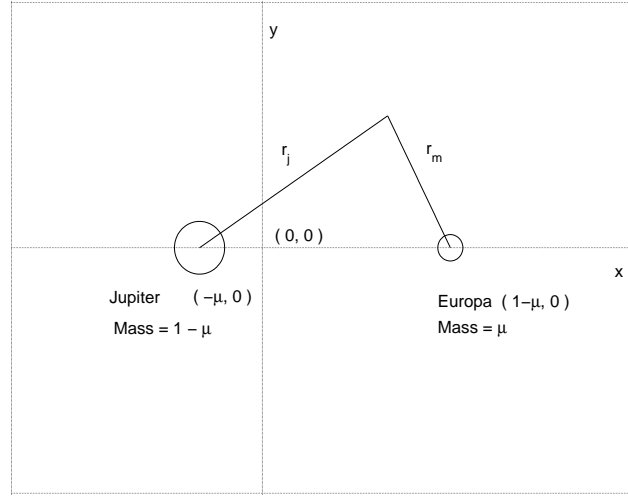


**Figure 1: Jupiter-Europa schematic**

The normalized values of the masses and equatorial radii for Jupiter and Europa are summarized in Table 1 and correspond to the following values for the parameters  $\mu$  and  $\nu$ :

$$\mu \simeq 2.52789 \times 10^{-5} \quad \text{and} \quad \nu \simeq 9.9998 \times 10^{-1}$$

Also, the distance between the two celestial bodies is approximately 671,000 km which corresponds to a normalized distance of one.

**Table 1: Normalized values for the masses and Equatorial radii of Jupiter and Europa**

	Mass	Equatorial Radius
Europa	$4.7998 \times 10^{22}$ kg	1565 km
Europa (normalized)	$2.5279 \times 10^{-5}$	$2.3323 \times 10^{-3}$
Jupiter	$1.8987 \times 10^{27}$ kg	71492 km
Jupiter (normalized)	$9.9998 \times 10^{-1}$	$1.0655 \times 10^{-1}$
Factor	$1.8988 \times 10^{27}$	$6.7100 \times 10^5$

In this normalized setting and rotating frame, the equations of motion can be expressed in coordinate form as:

$$\ddot{x} - 2\dot{y} - x = -\frac{\nu}{r_j^3}(x + \mu) - \frac{\mu}{r_m^3}(x - \nu) \quad (1)$$

$$\ddot{y} + 2\dot{x} - y = -\left(\frac{\nu}{r_j^3} + \frac{\mu}{r_m^3}\right)y \quad (2)$$

$$\ddot{z} = -\left(\frac{\nu}{r_j^3} + \frac{\mu}{r_m^3}\right)z \quad (3)$$

where  $r_j$  and  $r_m$  represent the distances from the spacecraft to Jupiter and Europa, respectively:  $r_j = \sqrt{(x + \mu)^2 + y^2 + z^2}$  and  $r_m = \sqrt{(x - \nu)^2 + y^2 + z^2}$ .

By setting  $z = 0$ , we obtain the equations of motion in the plane, with equation (3) reducing to  $\ddot{z} = 0$  and equations (1) and (2) having no  $z$  component.

## The Jacobi Constant, Zero Velocity Curves and equilibrium points

It can be shown that the above system is an autonomous Hamiltonian system and thus presents a first integral of motion (the Hamiltonian function). We define the Jacobi integral of motion,  $C$ , as minus twice the Hamiltonian function:

$$C = 2\Omega(x, y, z) - v^2$$

where  $v = \sqrt{\dot{x}^2 + \dot{y}^2 + \dot{z}^2}$  represents the speed of the particle and  $\Omega(x, y, z)$ , the effective potential, is defined as:

$$\Omega(x, y, z) = \frac{x^2 + y^2}{2} + \frac{\nu}{r_j} + \frac{\mu}{r_m}$$

This conservation law provides a connection between the displacement of the particle and its velocity for a given value of  $C$ ; increasing  $C$  will decrease this value. Since the velocity value cannot be negative, we have

$$v^2 = 2\Omega - C \geq 0.$$

Hence, for a particular value of  $C$ , motion is restricted to the region defined by  $2\Omega - C \geq 0$ , the boundary of which, called the zero-velocity curve/surface, is obtained by setting  $v = 0$  in the previous equation. It is thus implicitly defined by the equation  $f(x, y, z) = 2\Omega - C = 0$ , and depends on both  $C$  and  $\mu$ . Figure 2 shows an example of such a zero-velocity curve/surface. Any point  $(x, y, z)$  which evaluates to a negative value is unreachable at this particular energy level, and the set of such points is referred to as the forbidden region, with the zero-velocity curve serving as a boundary. The forbidden regions and corresponding velocity curves will be discussed further later in connection with our trajectory classification.

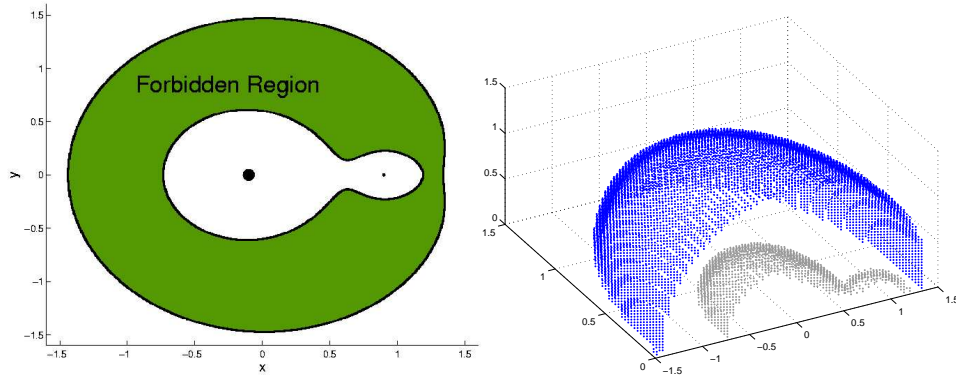


**Figure 2: Zero-velocity curve with  $C = 3.5$  and  $\mu = 0.1$ . (a) Planar case. (b) A partial 3D representation.**

Another important feature of the CR3BP is the existence of five equilibria, called the Lagrange equilibrium points, and denoted by  $L_1$  through  $L_5$ . At these points the gravitational fields of the two large celestial bodies perfectly balance the centrifugal force experienced by the “massless” third body. These equilibrium points are of interest since at these points the Jacobi constant takes critical values for which the dynamics of the system changes and will thus help in the classification of the set of trajectories considered in the following. The Lagrange points are also the source of stable and unstable manifolds that will shed some light in the results obtained. The coordinates of the Lagrange points for the Jupiter-Europa system and the corresponding energy levels are listed in Table 2 and a visual representation of their location can be seen in Figure 2.

## COMPUTATIONAL FRAMEWORK

The numerical investigation of the flow of trajectories leaving the surface of Europa proceed by sampling the initial condition space restricted to the surface of Europa at a given value of the Jacobi energy, and integrating these conditions forward in time until impact with Europa or Jupiter occurs or a given time has elapsed. This approach can be

**Table 2: Coordinates for Lagrange points in Jupiter-Europa system**

	$x$	$y$	$C$
$L_1$	0.97976	0	3.00364
$L_2$	1.02047	0	3.00361
$L_3$	-1.00001	0	3.00003
$L_4$	0.44997	0.86603	2.99997
$L_5$	0.44997	-0.86603	2.99997

viewed as a single iterate of a Poincaré map whose surfaces of section are defined by the physical surface of Jupiter and Europa (approximated as spheres). The set of trajectories leaving Europa is thus homeomorphic to  $S^1 \times D^1$  in the planar case and  $S^2 \times D^2$  in the 3D case. This section describes in further detail the parameterizations used as well as the dynamical characteristics of the trajectories considered.

### Surface of section parameterization

The first step for the computation of the Poincaré maps consists in finding a parameterization for the space of initial conditions. In the planar case, this space is 2D and can be parameterized by two angles  $\alpha$  and  $\beta$ :  $\alpha$  determines the launching position on the moon and  $\beta$  determines the launching direction measured from the tangent to the sphere. The parameterization is shown in Figure (a).

Using the relation between the Jacobi constant and the velocity given in the previous section, the  $x$  and  $y$  components of the initial position on the surface of Europa,  $x_0$  and  $y_0$  respectively, and the  $x$  and  $y$  components of the initial velocity,  $u_0$  and  $v_0$  respectively, relate to  $\alpha$  and  $\beta$  by the following equations:

$$x_0 = r_m \cos \alpha \quad ; \quad u_0 = v_i \cos \left( \alpha + \beta - \frac{\pi}{2} \right) \quad (4)$$

$$y_0 = r_m \sin \alpha \quad ; \quad v_0 = v_i \sin \left( \alpha + \beta - \frac{\pi}{2} \right) \quad (5)$$

where  $v_i = \sqrt{2\Omega(x_0, y_0) - C}$  is obtained from the definition of the Jacobi constant.

In the three dimensional model the surfaces of section are four dimensional and four parameters are required to fully specify the initial conditions. Treating the surface of Europa as a sphere, the launching position is given by two angles:  $\alpha$  ( $0 \leq \alpha < 2\pi$ ) is the rotation about the  $z$ -axis in the  $x$ - $y$  plane counted from the  $x$ -axis (right ascension), while  $\delta$  ( $-\frac{\pi}{2} \leq \delta < \frac{\pi}{2}$ ) is the angle of inclination from the  $x$ - $y$  plane (declination). Similarly, two angles specify the direction of the launching velocity. Specifically denoting  $(\mathbf{u}_1, \mathbf{u}_2, \mathbf{u}_3)$  the orthonormal basis obtained from the initial bases (that determines the  $x, y, z$  axis) after applying the above two rotations,  $\gamma$  ( $-\pi/2 \leq \gamma < \pi/2$ ) is the rotation about the  $-\mathbf{u}_2$  axis, while  $\beta$  ( $0 \leq \beta < \pi/2$ ) denotes the angle from the  $-\mathbf{u}_2$  axis to the velocity vector (con-

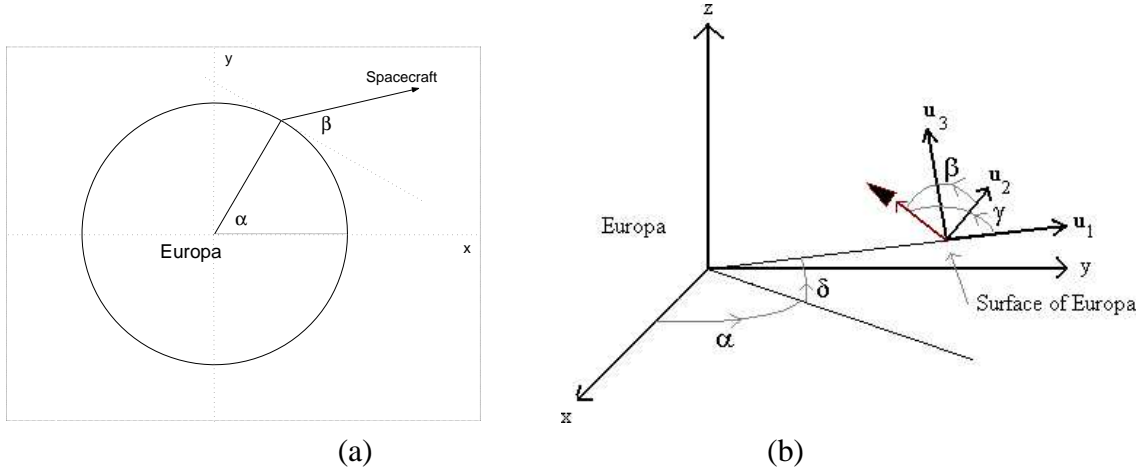


**Figure 3: Parameterizing the initial Europa launch conditions: (a) planar case, (b) 3D case.**

tained in the  $\mathbf{u}_1, \mathbf{u}_2$  plane after the above rotation). The parameterization is summarized in Figure (b).

Denoting, by  $R_3(\theta)$  and  $R_2(\theta)$  the rotations about the current  $z$  and  $y$  axis respectively<sup>‡</sup> and  $\mathbf{e}_1 = (1, 0, 0)$ , the initial conditions are given by the following relations:

$$\begin{pmatrix} x \\ y \\ z \end{pmatrix} = r_e R_3(-\alpha) R_2(\delta) \mathbf{e}_1 \quad \text{and} \quad \begin{pmatrix} \dot{x} \\ \dot{y} \\ \dot{z} \end{pmatrix} = v R_3(-\alpha) R_2(\delta + \gamma) R_3(\pi/2 - \beta) \mathbf{e}_1 \quad (6)$$

where  $r_e$  is the radius of Europa and  $v$  is the magnitude of the launching velocity (obtained from the Jacobi constant).

## Sampling algorithm and computation of the maps

After the space of initial conditions has been parameterized by two angles, the next step consists of choosing an algorithm to carry out the computation. The simplest approach to generate the Poincaré maps is the point-wise sampling algorithm: the parameter space is divided into a regular grid, with each grid point corresponding to an initial condition (using the relations presented in the previous subsection) for the subsequent numerical integration<sup>§</sup>. This numerical integration is performed over a specified time span  $T$ , unless an impact occurs with Jupiter or Europa<sup>¶</sup> and several dynamical criteria are then estimated

$${}^{\ddagger} R_3(\theta) = \begin{pmatrix} \cos \theta & -\sin \theta & 0 \\ \sin \theta & \cos \theta & 0 \\ 0 & 0 & 1 \end{pmatrix} \quad R_2(\theta) = \begin{pmatrix} \cos \theta & 0 & -\sin \theta \\ 0 & 1 & 0 \\ \sin \theta & 0 & \cos \theta \end{pmatrix}$$

<sup>§</sup>Numerical work presented in this paper has been performed using the MATLAB software, the numerical integration using the built-in ODE solver ode45.

<sup>¶</sup>The stopping condition for the impact condition has been realized via the MATLAB's *event* function.

along each trajectory (such as, the number of revolutions or the full state at impact). The resulting property values are then represented over the initial condition space (the parameter space), resulting in a map of the dynamics. While several dynamical properties have been computed, only the association of the initial condition with the property of impacting or not impacting Jupiter or Europa has been investigated in some depth.

In summary, in the 2D case, for each given pair of angles,  $\alpha$  and  $\beta$ , and a given Jacobi constant,  $C$ , the equations of motion may be integrated over a specified time span to arrive at a final state. The Poincaré map is obtained by discretizing of some chosen dynamical properties of the path taken and plotting these against the plane spanned by the angles of initial conditions. Figure 4 shows a sample Poincaré map over the full phase space. If viewed in color<sup>||</sup>, the red color correspond to impact with Jupiter, the blue color to impact with Europa, and the white color to no impact over the considered time span.

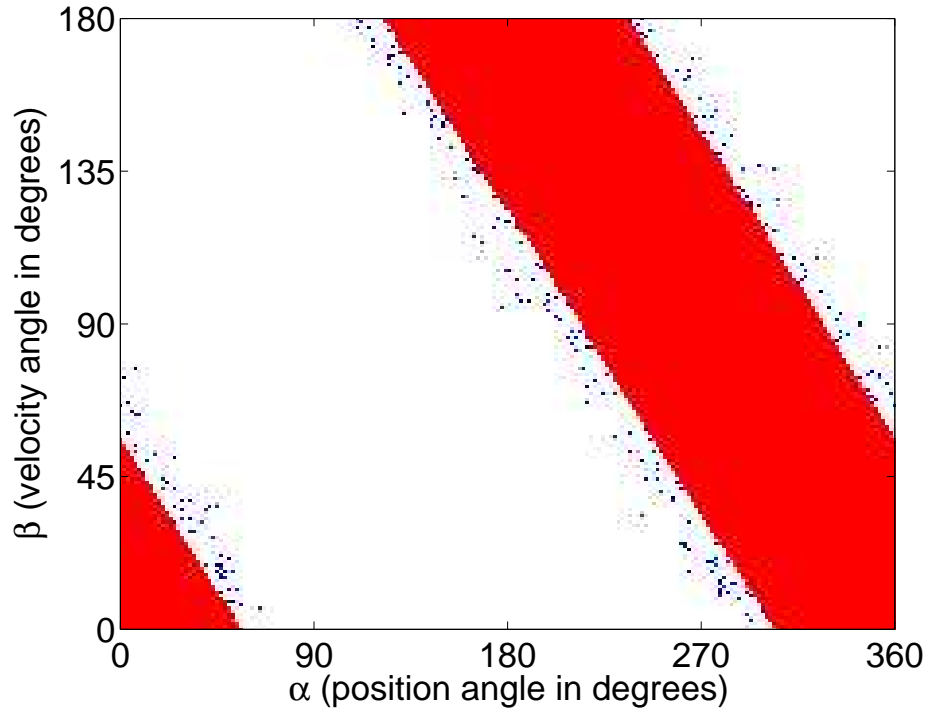


**Figure 4: Sample Poincaré map of the planar Jupiter-Europa system with  $C = 2.00$  and  $Time = 200$ . (Red: impact with Jupiter; Blue: impact with Europa; White: no impact over the given time span.)**

Similarly, in the 3D case, for each given quadruplet of angles  $(\alpha, \beta, \delta, \gamma)$  and a given Jacobi constant,  $C$  the equations of motion may be integrated over a specified time span to arrive at a final state. Again, the Poincaré map is obtained by discretizing some chosen

<sup>||</sup>If viewed in black and white, the dark strips correspond to crashing into Jupiter, the dark spots with crashing into Europa, and the white regions with no impact.

dynamical properties of the path taken and plotting these against the plane spanned by the angles of initial conditions. The difficulty with the Poincaré Map thus obtained is that it is 4 dimensional which makes the visualization more complex. One approach is to take either two or three dimensional slices to at least plot subsections of the full map. In particular, the case  $\gamma = 0$  and  $\beta = \frac{\pi}{2}$  corresponds to launching the orbiter in the direction normal to the surface of the moon. Hence, varying  $\alpha$  and  $\delta$  while fixing  $\gamma = 0$  and  $\beta = \frac{\pi}{2}$ , a 2D Poincaré map may be obtained to investigate the dynamics when the orbiter is projected normally to the surface of the moon at different locations. Alternatively, setting  $\gamma = \pm\pi/2$  and  $\beta = 0$  or  $\pi$ , one obtains the set of trajectories tangent to the surface of Europa, which is an approximation of the set of transfer trajectories of a low altitude Europa orbiter using tangential impulsive maneuvers at a periapsis<sup>10</sup>. Finally, setting  $\delta = 0$  and  $\gamma = 0$  removes the  $z$ -component of the velocity and position, resulting in the planar case presented above.

## NUMERICAL INVESTIGATIONS

This section presents the numerical results obtained using the point-wise algorithm when the time span and Jacobi constants are varied. A first explanation of the global features appearing on the Poincaré maps, provided by the constraint imposed by the zero velocity surfaces is discussed.

### Effect of the integration time

The definition of the computational algorithm in the previous section imposes one important numerical constraint: besides the inherent errors due to the approximate numerical computations (floating point representation by computers and finite order integration algorithm) the numerical estimation of the maps is limited by the integration time span  $T$ . Figure 5 shows a portion of the same Poincaré section (at an energy value corresponding to Figure 4) for two different time spans.

Figure 5 illustrates how the stripes corresponding to the impact with either Jupiter or Europa slowly appear as the time span increases, leaving stripes of no impact in between. Thus as the integration time interval increases more and more details become available, resulting in thinner and thinner connected regions with the same impact characteristics in the chaotic regions of phase space (mixing properties). However, at the scale length scale presented, a time span of  $T=200$  ( where  $T$  is measured in the normalized time units introduced in the first section) already presents much of the finer dynamics and seems sufficient for the purpose of this work.

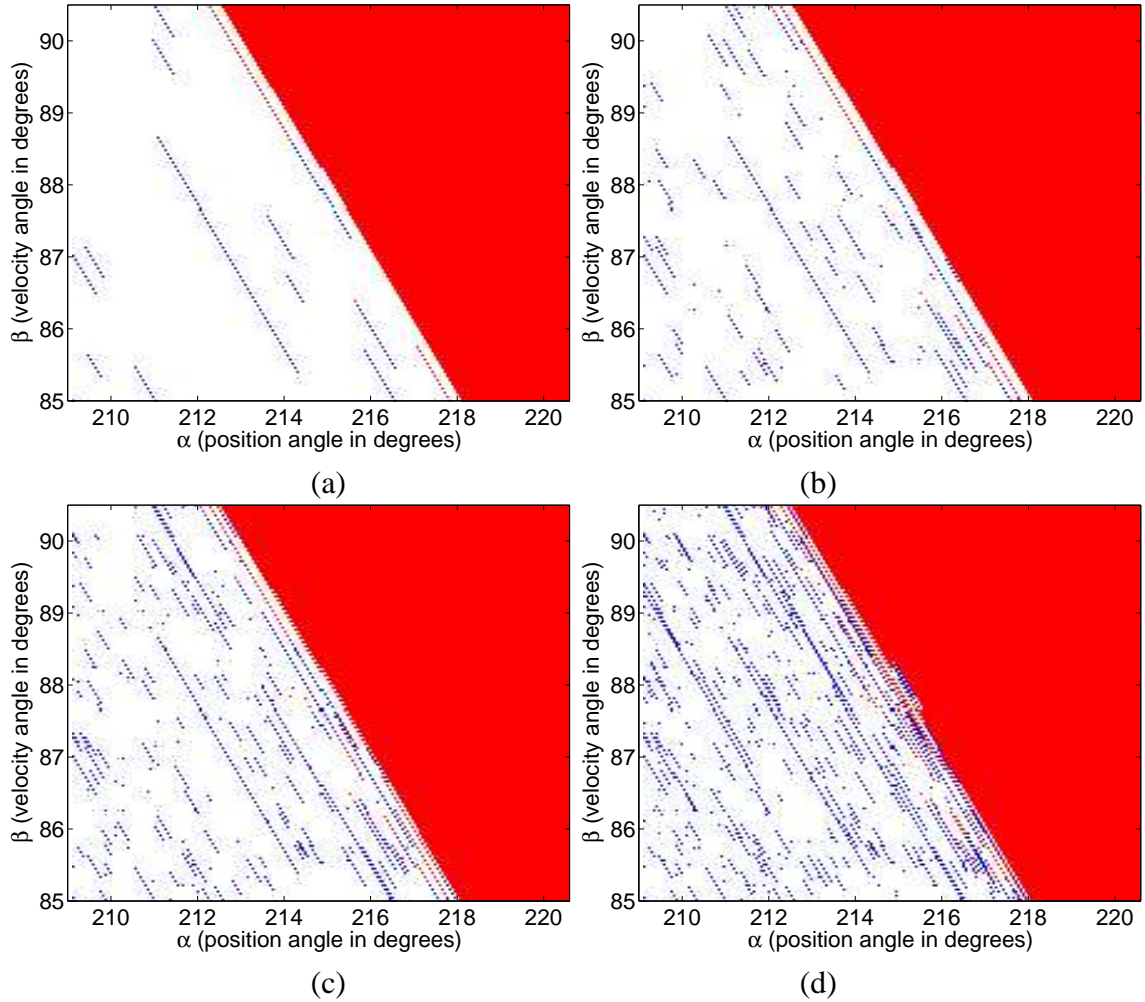


**Figure 5: Zoom near the boundary region of the main Jupiter impact strip, after a time span of (a) 50, (b) 100, (c) 150, and (d) 200. (Color code: Red corresponds to impact with Jupiter, Blue to impact with Europa and White with no impact over the time span considered.)**

### Variations with the Jacobi constant

The second major parameter entering the computational algorithm is the value of the Jacobi constant. Figures 6 and 7 present a series of Poincaré maps in the planar problem for several values of this parameter, together with a graph of the zero velocity curves associated with the same energy level\*\*. These curves give us a first understanding of the features observed on this maps. Indeed, the zero-velocity curves provide boundary conditions for possible trajectories of a spacecraft given a particular energy value. If the energy level is

---

\*\*The graph is presented with a larger value of  $\mu$  than the Jupiter-Europa system so that the moon regions can be viewed more clearly, but the exact same scenario applies to the Jupiter-Europa system, with the critical values of the *Jacobi constant* given in section .

too low (for a high value of  $C$ ), the forbidden region divides our space so that a spacecraft cannot travel between the two celestial bodies. For example, at such an energy level, a projectile launched from Europa would never be able to reach Jupiter or escape away from the moon and will most likely impact the moon, as seen on Figure 6(a).

A reduction of  $C$  corresponds to an increase of the energy of the system which leads to a contraction of the forbidden regions. Figure 6(b) shows the forbidden region opening up at the  $L_1$  equilibrium point. Starting at the critical Jacobi constant value  $C_1$ , the spacecraft can now reach the domain dominated by Jupiter's gravity field and some of the initial conditions result in non-impacting trajectories with Europa. However, at these low energies, no impact with Jupiter is observed.

With another small decrease in the value of  $C$ , the zero velocity curves now open at the  $L_2$  equilibrium point, and a larger set of trajectories are allowed to exit the Europa sphere of influence, as shown in Figure 6(c). As we can see the set of non-impacting conditions increased in such a way as to form two tongues with mixing of impacting and non-impacting trajectories.

A further reduction of  $C$ , as shown on Figure 7(a), leads to a widening in the opening of the zero velocity curve and the corresponding increase in the set of non-impacting trajectories. This evolution lead to the concentration of the impact condition along several distinct stripes of slope close to  $-1/2$ .

Decreasing yet further the value of  $C$ , the zero velocity curve breaks into two disjoint components at  $L_3$ , allowing trajectories to escape the system through  $L_3$  (Figure 7(b)). The tendency of the set of non-impacting trajectories to grow continues and becomes in fact the dominant behavior at this energy; however, no impact with Jupiter appears at this  $C$  value.

Finally, the forbidden region vanishes at the final two equilibrium points,  $L_4$  and  $L_5$ , as shown on Figures 7(c). In this case, a spacecraft is free to move anywhere in position space and the set of Europa impacting trajectories now concentrate into a single strip of slope  $\sim -1$ , starting around  $\alpha = 360^\circ$  and  $\beta = 0^\circ$ . Yet, at the energy considered on this Figure, no impact with Jupiter is observed. Lower values of  $C$  are required for the appearance of a Jupiter impact, as was shown in Figure 4.

Thus we can see that, even though the dynamics switch from one dominated by the gravitational field of Europa at higher values of the Jacobi constant (Figure 6a) to a dynamics dominated by Jupiter at lower values of  $C$ , where a large stripe of initial conditions impacting with Jupiter appears as the main feature (Figure 4), the transition between these two cases presents very complex dynamics. Besides some kind of randomness in the distribution of impact locations with Europa, there are still some global features that can be identified.

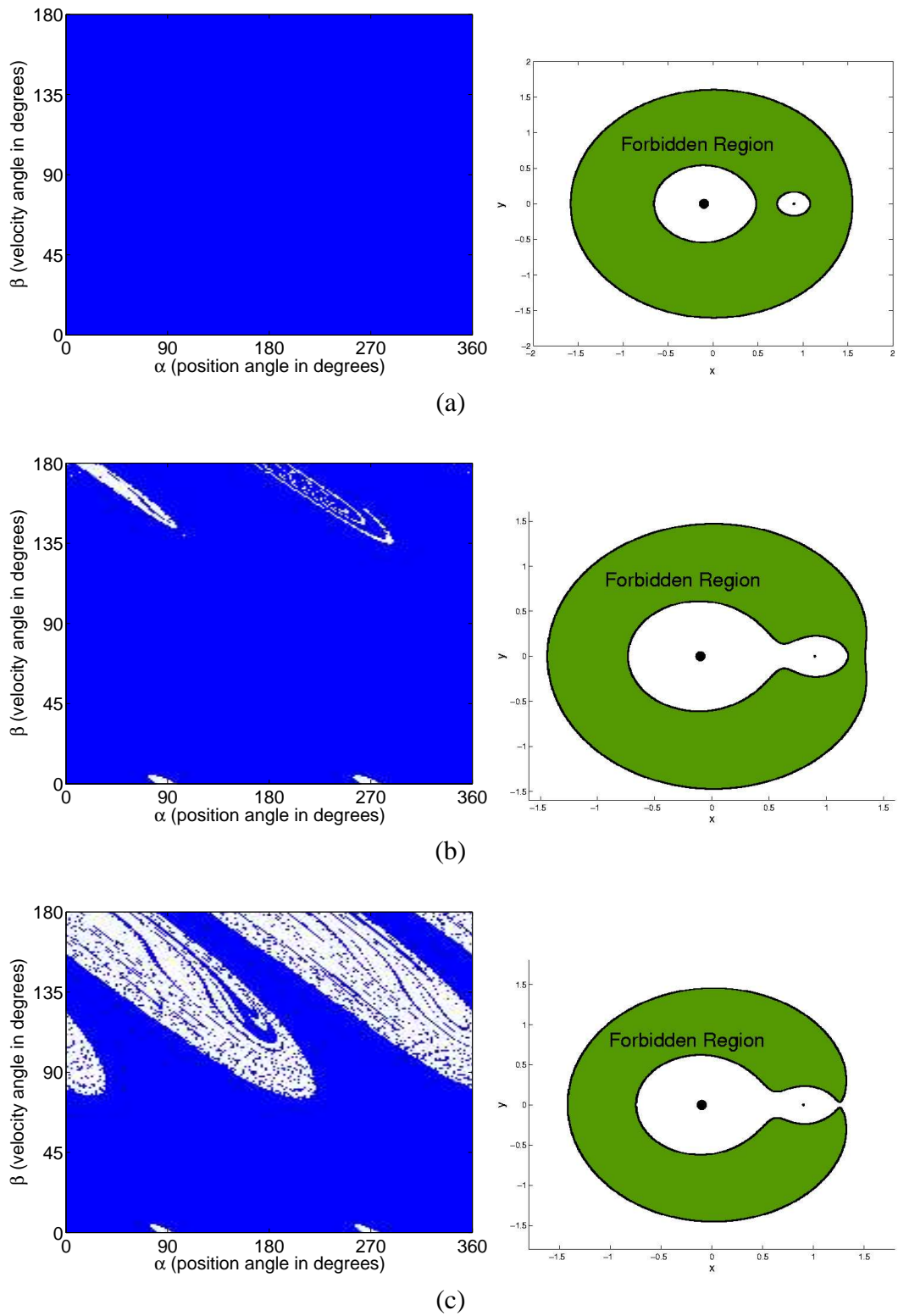


**Figure 6:** Sequence of Poincaré maps (left column,  $T = 200$ ) with corresponding zero velocity surface (right column) for a Jacobi constant value of (a) 3.1, (b) 3.00362, (c) 3.003.

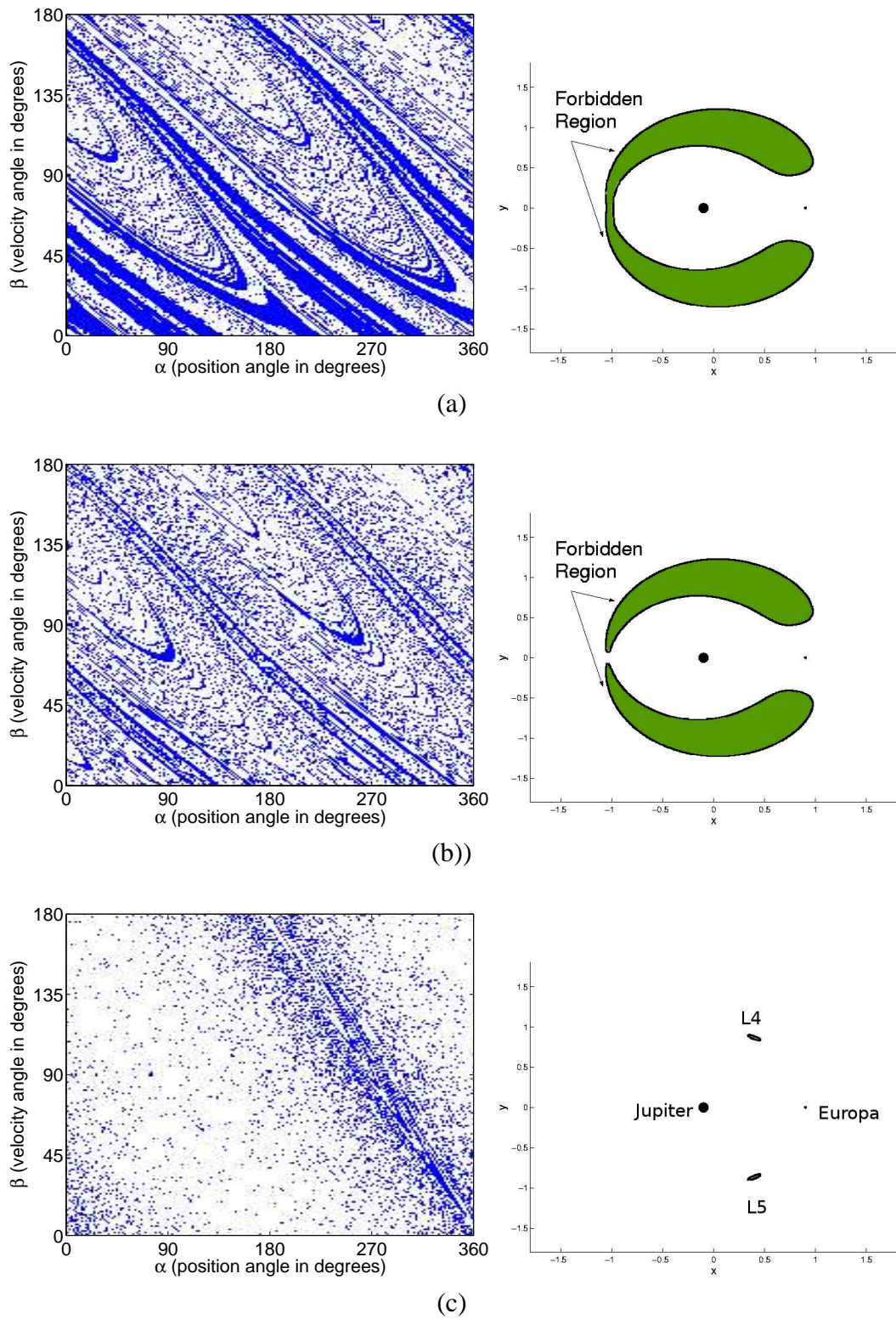


**Figure 7: Sequence of Poincaré maps (left column,  $T = 200$ ) with corresponding zero velocity surface (right column) for a Jacobi constant value of (a) 3.001, (b) 3.0, (c) 2.9.**

## THEORETICAL EXPLORATIONS

While the zero velocity surface gives a first glimpse into the dynamics of our Poincaré maps, it does not explain the shape of the non-impact trajectories at low energies, nor the affine nature<sup>††</sup> and location of the main impact stripes with Jupiter that appear at higher energies. In this section, we explore two approaches to answer such questions.

### Invariant manifold theory

The stable and unstable manifolds associated with the periodic and quasi-periodic trajectories present in the vicinity of the colinear libration points have recently played a key role in mission design such as the Genesis mission<sup>5</sup>. In fact, it has been shown by Conley<sup>1</sup> that these manifolds form the boundary between transit and non-transit orbits<sup>‡‡</sup> for low energies and Lo proposed the concept of Inter-Planetary Superhighways<sup>6</sup> associated with these dynamics. These stable and unstable manifolds thus represent a natural theoretical framework to analyze the computed dynamical maps. This subsection investigates their ability and limits to capture the dynamics observed.

*Brief review of the theory.* In the PCR3BP, the dynamics in the vicinity of the colinear libration points is homeomorphic to a center  $\times$  saddle, where the center part generates the family of Lyapunov periodic orbits while the saddle part gives rise to the unstable character of the dynamics.

The stable manifolds associated with the Lyapunov periodic orbits are formed by the set of trajectories converging to the periodic orbits in forward time, whereas the unstable manifolds are formed by the set of trajectories converging to the periodic orbit in backward time.

Numerically these sets of trajectories can be approximated by computing the stable and unstable eigen-directions associated with the monodromy matrices<sup>†</sup> of a sequence of points along the periodic orbit. The steps for approximating these manifolds are thus as follows:

1. Given initial conditions for a periodic orbit, generate a sequence of points around the periodic orbit by propagating the initial condition.
2. For each point, calculate the monodromy matrix and operate a small displacement along the unstable eigen-direction direction of the monodromy matrix to arrive at a set of points slightly off the periodic orbit.

---

<sup>††</sup>That is the boundaries of these regions seem well approximated by straight lines.

<sup>‡‡</sup>Transit being understood as transfer from a region gravitationally dominated by Europa to a region of phase space dominated by Jupiter, or vice versa.

<sup>†</sup>We recall that the monodromy matrix associated with a point of a periodic orbit is the name given to the State Transition Matrix when evaluated after one period. The stable directions are determined by the eigenvectors whose corresponding eigenvalue is less than one, while the unstable eigen-directions are associated with the eigenvalues greater than one.

3. Take each point in the set as an initial condition and integrate the path to generate a tube of trajectories.
4. Use the time symmetry in the PCR3BP model to derive the stable manifolds from the unstable manifolds.

We should like to point out that this procedure has been found to be rather sensitive to numerical inaccuracies and parameters (e.g. offset along the eigen-directions) and small integration tolerance ( $\simeq 10^{-12}$ ) have been used.

Figure 8(a) presents the projection onto the  $x$ - $y$  plane of a set of trajectories approximating the stable and unstable manifolds of a Lyapunov periodic orbit near  $L_1$  at  $C = 3.00362$ . The periodic orbit can be distinguished in the center of the figure where the manifold tubes intersect. The branch of the stable manifold coming from the Europa region (right of the Lyapunov orbit in Figure 8(a)) will be referred to as the positive branch, while the negative branch will refer to the branch coming from the Jupiter region (left of Figure 8(a)).

Figure 8(b) shows a more extended view of this 2D projection. The negative branches of the manifolds wind around Jupiter and stay rather close to the zero velocity curve, while the positive branches intersect the surface of Europa (feature not apparent at the scale of the Figure).

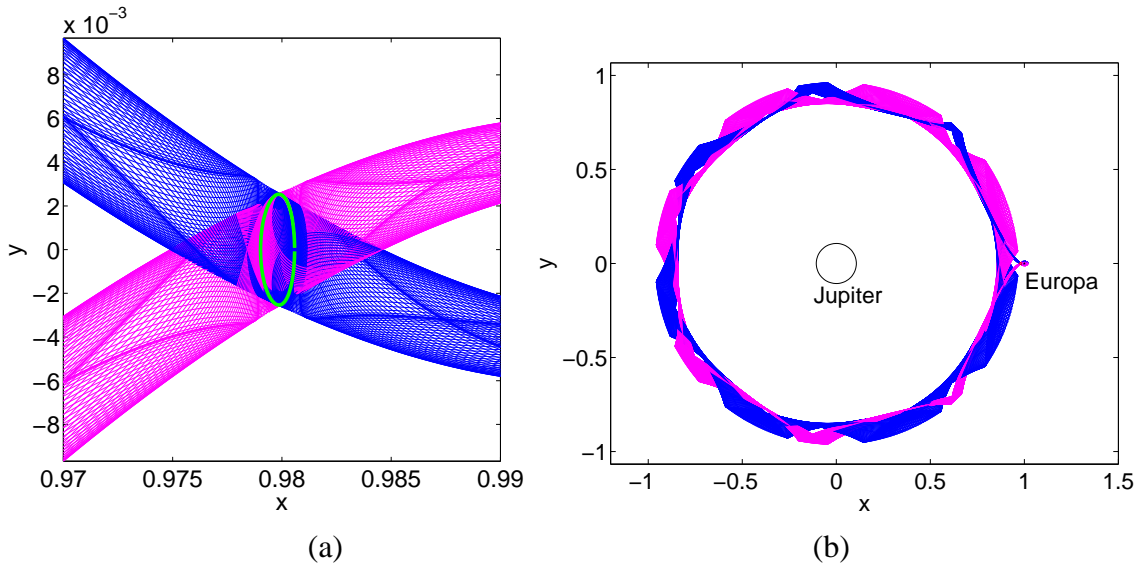


**Figure 8: Projection of set of trajectories approximating the stable (pink color) and unstable (blue color) manifolds of an  $L_1$  Lyapunov orbit onto the  $x$ - $y$  plane: (a) Zoom near the  $L_1$  Lyapunov periodic orbit, (b) Global projection. The positive branches of the manifolds lie on the left of the Lyapunov orbit in (a), while the negative branches lie to its right.**

The stable and unstable manifolds are in fact homeomorphic to certain tubes in phase space that separate different types of motion. By analyzing the linearized dynamics around

the colinear libration points, Conley<sup>1</sup> was able to prove that these stable and unstable manifolds separate the sets of transit and non-transit trajectories. The transit trajectories lie inside the tubes formed by the manifolds whereas the trajectories outside these tubes stay forever in the vicinity of a single primary.

*Application to the dynamical maps.* The idea that the manifolds can be viewed as boundaries in the flow of trajectories between sets of trajectories leaving the Europa region and sets of trajectories remaining in the Europa region is of great use for understanding of structure of the Poincaré maps. This fact indeed suggests that the sets of non-impacting trajectories present for example in Figure 6(b) may be bounded by the stable manifolds associated with the Lyapunov orbits present at the energy considered. By calculating the intersection of the stable manifolds with the surface of Europa it is possible to partition the Poincaré map according to whether the particle leaves the Europa region or not. The particle launched from the surface of Europa can travel to the Jupiter region if and only if the initial launching position on Europa is inside the intersection of the surface of Europa with the stable manifold. In particular, on the Poincaré map, all the initial conditions on Europa leading to impact with Jupiter must be bounded by points corresponding to the impact conditions of the manifold with the surface of Europa. Figure 9 shows the Poincaré map presented in Figure 6(b) with the addition of some intersection points of the stable manifolds originating from the periodic orbit around  $L_1$  with the surface of Europa.

The Poincaré map shows that the intersections of the stable manifolds with the surface of Europa lie indeed at the boundary between the sets of impacting/non-impacting trajectories lying in the upper-part of the dynamical map, thus validating in part the above theoretical suggestion. The distinction between the positive and negative branches or the stable manifold shows that an outer envelope of the set of non-impacting trajectories is provided by the positive branch of the stable manifold (coming from the Europa region), while the structure between the sets of impacting/non-impacting trajectories inside this outer envelope is provided by the negative branch of the stable manifold (coming from the Jupiter Region). In particular, this shows that the trajectories impacting Europa but lying inside the outer envelope makes at least one revolution around Jupiter before impacting. This is not the case for the other impacting trajectories that stay in the Europa region between launch and impact. Finally, we note that the intersection of the manifolds appears in two different places on the Poincaré map since for this energy value, the manifolds do not intersect the surface of Europa directly. Instead, they wind around Europa several times and scrape the surface at different places, progressively impacting in different regions, as shown in Figure10.

As a manifold impacts the surface, the trajectories just avoiding Europa are tangent of Europa. Thus the different regions of intersection are either bounded by manifolds or by the lines on the Poincaré map corresponding to  $\beta = 0$  or  $\beta = 2\pi$  at which the trajectories are tangent to the surface. In fact, it is observed at these energies that the crossings of the manifolds are always in the direct sense of motion., that is for  $\beta > \pi/2$  (Equation (5)). The set of non-impacting trajectories lying close to  $\beta = 0$  in the above Figure, are not associated with these libration point dynamics as they represent retrograde trajectories.

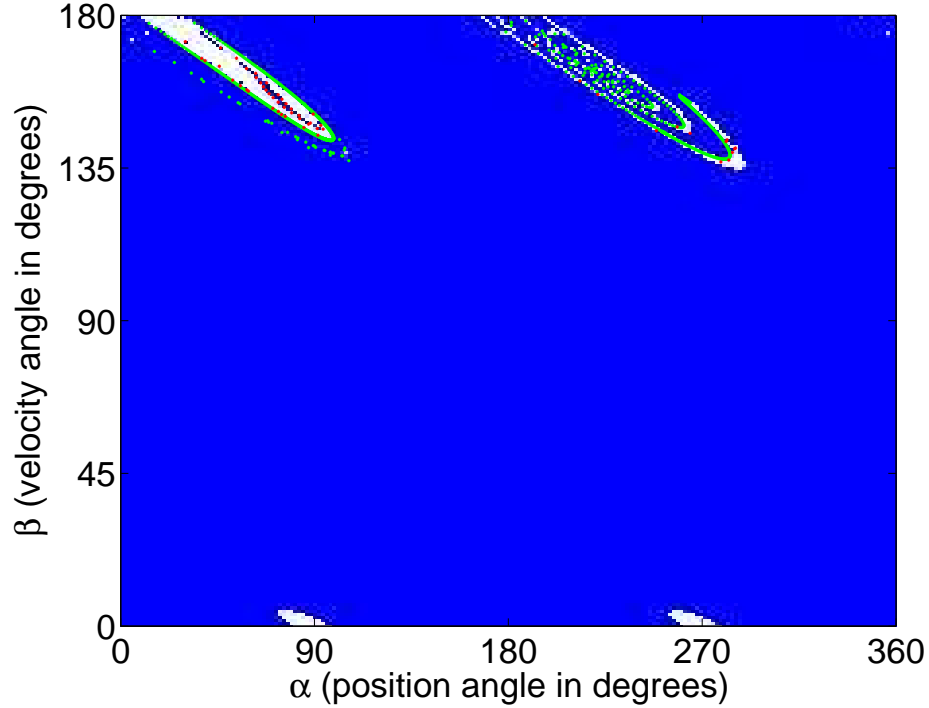


**Figure 9: Intersection of the stable manifold with Europa (red dots), reported on the dynamical map corresponding to the same energy value,  $C = 3.00362$ . The color code for the dynamical map is the same as in Figure 6: blue color for impact with Europa and white for non-impacting trajectories. The stable manifold cuts are seen to lie at the boundary of some thin regions of non-impacting trajectories. The green dots represent the intersection of the positive branch of the manifold with Europa, while the red dots represent the intersection of the negative branch.**

These trajectories leave the surface of Europa but do not reimpact Europa over the given time span. In fact, this set shrinks to the null set as the time of integration is increased. This set of trajectories has a longitude of periapsis close to  $\pi/2$  and  $3\pi/2$  and corresponds to regions of phase space where the perturbations tend to raise the periapsis radius.

Finally, we should like to point out that the absence of impact trajectories with Jupiter for low energies is readily explained using the invariant manifold theory. Indeed, as we have seen on Figure 8(b), the path of the invariant manifolds stays away from Jupiter. This has been proved to hold for all times for low values of  $C$  by McGehee<sup>7</sup>. From the manifold theory, we know that all the trajectories leaving the influence of Europa are bounded by these invariant tubes so that no impact with Jupiter appears possible. While the manifolds have only been computed for very low energies, Figures 6 and 7 show that such a situation holds for a larger range of energies. The computation of the invariant manifolds at these energies become however much more intricate as more and more intersections between these manifolds result in chaotic dynamics, as is especially apparent on Figure 7.

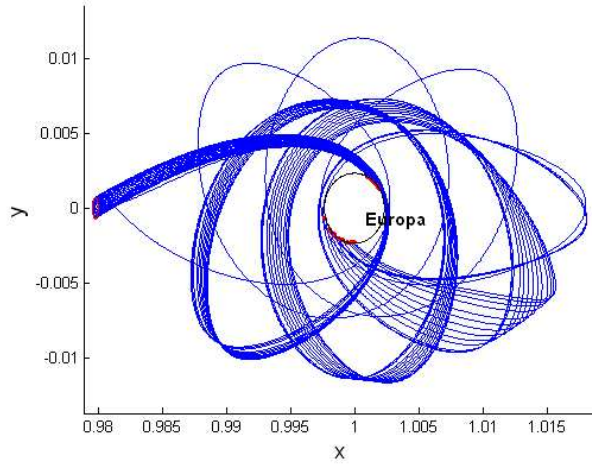


**Figure 10: 2D projection of a stable manifold and its intersection with Europa.**

## Two-Body Model Approximation

The above invariant manifold theory allows us to capture important features of the dynamical maps generated but does not seem appropriate to easily characterize the main impact stripes with Jupiter, observed at high enough energies (Figure 4). In this subsection, we investigate such features by approximating the equations of motion by a two body problem. This approximation is obtained by letting  $\mu \rightarrow 0$  in the equations of motion (Eq. 5), and is physically justified for high enough energies since the large velocity at the surface of Europa implies that the ejected particles will quickly escape the attraction of Europa and will be dominated by the gravitational field of Jupiter. This is even more so for small moons where the mass ratio  $\mu$  is very small. This effect of quick escape from the primary is also modeled by also letting the radius of the moon  $R_E \rightarrow 0$  with the mass ratio  $\mu$ .

*Dynamical Reduction.* First, we observe that by letting the radius of the planetary satellite go to zero, the surface of the moon shrinks to a single point and the position angles that parameterize this surface do not make sense any more. Thus, in the limit, the orientation of the velocity is the only parameter of the Poincaré map (besides the energy). Thus in the two dimensional case, the dynamical maps computed should depend on only a single parameter, as this explains the affine nature of the observed main impact stripes with Jupiter at high energies (Figure 4). Indeed, in this case, denoting  $\theta$  the orientation of the velocity vector from the  $x$ -axis, the parameterization (5) yields the relation:

$$\theta = \alpha + \beta - \pi/2 \quad (7)$$

that is, all the point on the dynamical maps (at a fixed value of  $C$ ), for which  $\alpha + \beta - \pi/2$  is a given constant, should have the same dynamical properties. The equation (7) represents a one dimensional family of parallel lines of slope  $-1$ .

In the three dimensional problem, the algebraic relation is a little more involved, but

the idea remains the same. As  $R_E \rightarrow 0$ , the dynamics on the maps considered vary only with the velocity orientation, which in this case can be parameterized by the right ascension and declination of the velocity angle in the rotating frame centered at the moon. Using the equations (6), we see that all the points  $(\alpha, \delta, \beta, \gamma)$  on the dynamical maps for which the following relation hold ( $\theta_1$  and  $\theta_2$  held constant):

$$\begin{aligned}\cos \alpha \sin \beta \cos (\delta + \gamma) - \sin \alpha \cos \beta &= \cos \theta_2 \cos \theta_1 \\ \sin \alpha \sin \beta \cos (\delta + \gamma) - \cos \alpha \cos \beta &= \cos \theta_2 \sin \theta_1 \\ \sin \beta \sin (\delta + \gamma) &= \sin \theta_2\end{aligned}$$

should have the same dynamical properties (for any given, but small enough value of  $C$ ).

These arguments allow us to conclude that the global variations of the 2D dynamical maps as a function of  $C$  and  $\theta$  should be representable on a single graph, while global dynamics on any given 4D dynamical maps (for high enough energy), should be representable on a 2D graph. The next subsections investigate these variations for the impact/non-impact dynamics.

*Impact with Jupiter.* The location of the impact strip on the Poincaré section can be obtained by analyzing the concept of periapsis (or perijove, point of closest approach from Jupiter) in the two body approximation. Indeed, denoting  $r_p$  as the radial distance of this perijove, impact with Jupiter will occur only if  $r_p \leq R_J$ , where  $R_J$  denotes the radius of Jupiter. This necessary condition is sufficient for elliptic motion, while one must also consider the condition  $\dot{r} < 0$  at the initial point for parabolic and hyperbolic motion<sup>‡</sup>.

When considering these dynamics in the rotating frame, the velocity corrections due to the rotating nature of the frame must be taken into account. More precisely, denoting  $\mathbf{v}_i$  the velocity in the inertial frame centered at Jupiter,  $\mathbf{v}_r$  the velocity in the rotating frame and  $\boldsymbol{\omega} = (0, 0, 1)$  the angular velocity of the frame, we have:

$$\mathbf{v}_i = \mathbf{v}_r + \boldsymbol{\omega} \times \mathbf{r} = \begin{pmatrix} v_r \cos \theta \\ v_r \sin \theta + 1 \end{pmatrix} \quad (8)$$

where  $v_r$  represents the magnitude of  $\mathbf{v}_r$  and is obtained via the Jacobi constant (held fixed on the Poincaré section considered). More precisely, since in the limit  $\mu \rightarrow 0$ , all the Poincaré sections reduce to  $r = 1$ , the velocity  $v_r$  is given by<sup>§</sup>:

$$v_r = \sqrt{2r^2 + 2/r - C} = \sqrt{3 - C}$$

Thus, as the angle  $\theta$  is varied, the inertial velocity describes a circle of radius  $v_r$  around the point  $(0, 1, 0)$ , as illustrated in Figure 11.

<sup>‡</sup>For non-elliptic motion, only one periapsis exists and is simply determined by the condition  $\dot{r} = 0$ . It delineates two branches:  $\dot{r} < 0$ , the particle moves towards periapsis, and  $\dot{r} > 0$ , the particle escape towards infinity.

<sup>§</sup>Note that this assumes implicitly that we are looking at the dynamics for energies such that  $C < 3$  (i.e. the zero velocity surface is open up at  $L_1$  and  $L_2$ ).

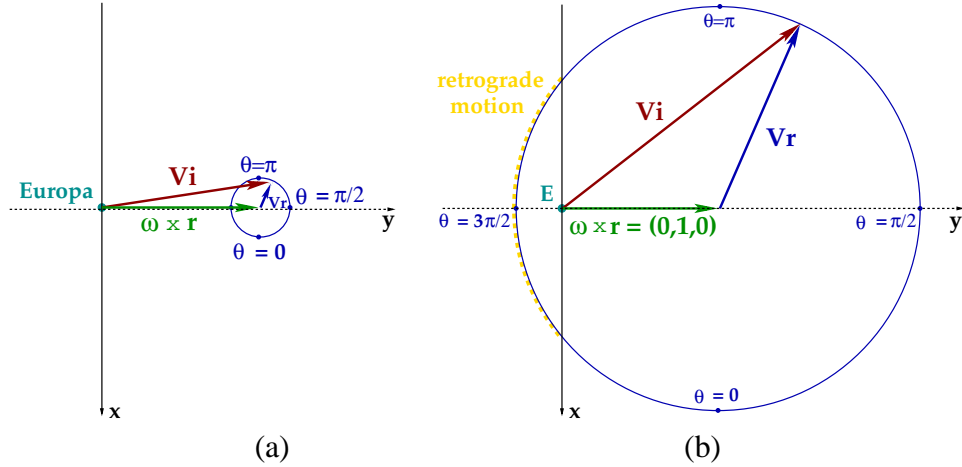


**Figure 11: Variation of the inertial velocity with  $\theta$  at constant  $C$ ; (a) For  $C$  close to 3, the set of inertial trajectories generated when  $\theta$  varies remains close to Europa's circular orbit. (b) For  $C$  greater than 2, some of the inertial trajectories generated are retrograde around Jupiter.**

For  $v_r$  close to 3, the radius of the circle described by the inertial velocity is small, so that the inertial velocity remains close to the vector  $(0, 1, 0)$  as  $\theta$  is varied. Since this velocity corresponds to a circular motion of radius 1 around Jupiter, no trajectories leaving Europa for  $C$  close to 3 will impact in the two body approximation<sup>¶</sup>. As the Jacobi constant is decreased, however, the inertial velocity circle increases, until the minimum value of  $v_i$  on that circle (reached for  $\theta = 3\pi/2$ ) corresponds to an impact, elliptic trajectory with Jupiter and a strip of impact points on the dynamical maps appears.

In order to obtain quantitative information on this first impact point, we note the impact condition  $r_p \leq R_J$  is equivalent to the condition  $f(E, h) \leq 0$  where the function  $f$  is defined as:

$$f(E, h) = h^2 - 2ER_J^2 - 2R_J \quad (9)$$

the coefficients  $E$  and  $h$  denoting the Keplerian energy and angular momentum magnitude of the spacecraft in inertial space, respectively<sup>||</sup>.

Now, since  $E = \frac{1}{2}v_i^2 - \frac{1}{r}$  and  $h = \mathbf{r} \times \mathbf{v}_i$ , we obtain:

$$E = 1 - C + \sqrt{3 - C} \sin \theta \quad (10)$$

$$h = (0, 0, v_r \sin \theta + r^2) \quad (11)$$

<sup>¶</sup>This shows that for low energies, the two body approximation is not a good approximation.

<sup>||</sup>Denoting  $v_p$  the inertial velocity at periapsis, we have  $h = r_p v_p$  and  $E = \frac{1}{2}v_p^2 - \frac{1}{r_p}$ , so that  $h^2 - 2Er_p^2 - 2r_p = 0$ . Subtracting this expression to the definition of  $f$  and using the relation  $r_p \leq R_J$ , the assertion can easily be checked.

which upon substitution in (9), results in:

$$f(C, \theta) = (3 - C) \sin^2 \theta + 2(1 - R_J^2) \sqrt{3 - C} \sin \theta + R_J^2(C - 2) - 2R_J + 1$$

This is a quadratic function of  $\sin \theta$  and is negative (i.e.  $r_p \leq R_j$ ), when  $\sin \theta$  lie in the interval,  $I(C)$ :

$$I(C) = \left[ -\frac{1 - R_J^2}{\sqrt{3 - C}} - R_J \sqrt{1 + \frac{\kappa}{3 - C}}, -\frac{1 - R_J^2}{\sqrt{3 - C}} + R_J \sqrt{1 + \frac{\kappa}{3 - C}} \right] \quad (12)$$

where  $\kappa = \frac{2}{R_J} - 3 + R_J^2 \simeq 15.78$ .

This condition gives us a complete picture of the condition  $r_p \leq R_j$  on the  $(C, \theta)$ -plane. In particular, the highest value of  $C$  for which impact is possible (in the two body approximation) is reached when  $\theta = \frac{3\pi}{2}$  and  $-\frac{1 - R_J^2}{\sqrt{3 - C}} + R_J \sqrt{1 + \frac{\kappa}{3 - C}} = -1$ , that is for  $C = 3 - \left(1 - R_J^2/2 + 0.5\sqrt{R_J^4 - 8R_J^2 + 8R_J}\right)^2 \simeq 2.6887$ . This is in agreement with the plots shown in Figure 7.

In order to complete the solution of the impact problem, we must solve for the condition  $E \geq 0$  and the condition  $\dot{r} < 0$ . The first condition is solved by noting that the variation of  $E$  with the Jacobi constant is a quadratic equation in  $\sqrt{3 - C}$ , so that the condition  $E \geq 0$  is equivalent to:

$$C \leq 3 - \left(\sqrt{\sin^2 \theta + 1} - \sin \theta\right)^2 \quad (13)$$

The condition  $\dot{r} < 0$  can be checked to be equivalent to  $\theta \in [\pi/2; 3\pi/2]$  for  $E \geq 0$  and these results can be represented graphically as a function of  $C$  and  $\theta$  as shown in Figure 12.

Note the existence of two distinct branches of the impact region once the Jacobi constant is small enough for the lower bound of the interval  $I$  to be greater than  $-1$ . That is, for  $C \leq C_{critical2} = 3 - \left(1 - R_J^2/2 + 0.5\sqrt{R_J^4 - 8R_J^2 + 8R_J}\right)^2 \simeq 0.95309$ , we have  $-\frac{1 - R_J^2}{\sqrt{3 - C}} - R_J \sqrt{1 + \frac{\kappa}{3 - C}} \geq -1$  and the impact strip is divided in two. A physical explanation comes from the variation of the inertial velocity with the velocity angle  $\theta$ . Looking at the points  $P^+(c)$  on the dynamical maps for which  $\theta = \pi/2$  (that is, a direct apsis), we see that a necessary condition for  $P^+(c)$  to be an impacting point is that it be an apoapsis\*\*. On the other hand, when the energy is increased, these points can become periapsis and no impact will occur. In fact, there is a range of  $C$  for which these points become periapsis, before the trajectories become non-elliptic. The same phenomenon happens for retrograde trajectories at  $\theta = 3\pi/2$  (points  $P^-(C)$ ), which was observed to exist in Figure 11(b). For  $C < 2$ , retrograde trajectories appear, but are impact trajectories for  $C$  close enough to  $2^{\dagger\dagger}$ . When  $C$  is increased, the apoapsis nature of these points will change to periapsis. This

---

\*\*That is, the farthest point on the orbit from Jupiter.

$\dagger\dagger$ Indeed, at  $\theta = 2\pi/2$  and  $C = 2$ ,  $\mathbf{v}_i = \mathbf{0}$  and the trajectory corresponds to a free fall trajectory, which is clearly impacting.

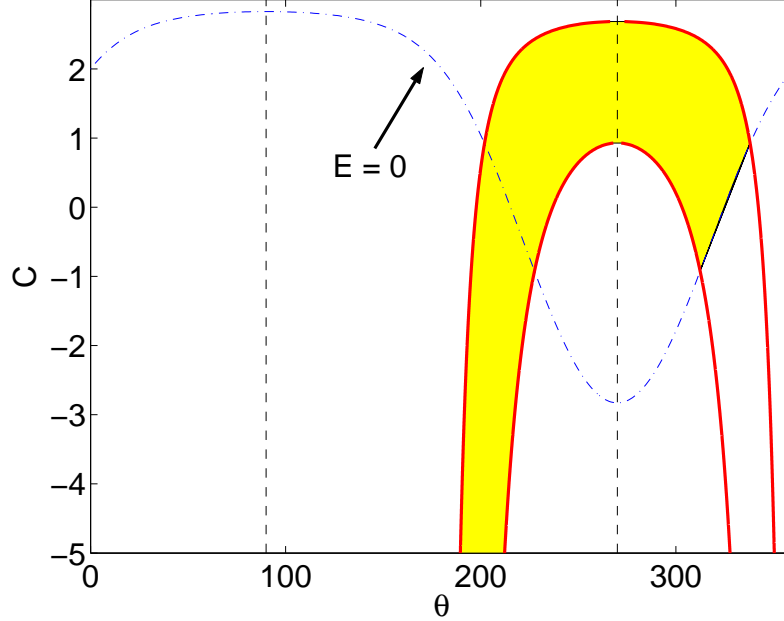


**Figure 12: Impact plot in a two body setting. The abscissa represents  $\theta$ , and the ordinate represent  $C$ . The region corresponding to impact condition is represented as the colored strip.**

change in apsis occurring when  $C$  is such that  $P^-(C)$  correspond to a retrograde circular orbit. For  $C$  just below that point, a small neighborhood around  $\theta = 3\pi/2$  will correspond to elliptic, non-impacting motion, while larger values of  $\theta$  will continue to result in impact with Jupiter.

Finally we should like to point out that the theory presented here in the two dimensional case works in the same way in the spatial problem. The periapsis condition  $r_p \leq R_J$  is still determined by  $f(E, h) \leq 0$ . The expression of this function in terms of  $C$  and the velocity angles  $\theta_1$  and  $\theta_2$  has the same form as in the planar case, except that  $\sin \theta$  is now replaced by  $\sin \theta_1 \cos \theta_2$ , so that the periapsis condition can be expressed as:

$$r_p \leq R_J \quad \text{if and only if} \quad \sin \theta_1 \cos \theta_2 \in I(C). \quad (14)$$

It should be noted that the  $(\theta_1, \theta_2)$  representation does match with the dynamical maps obtained when the initial velocity is taken as normal to the surface of Europa. The bifurcation observed in the planar case, now results in the transition from a disc-like impact region to an annulus-like impact region.

*Impact with Europa.* While the previous computation gives a complete answer for the approximation of the stripes, one can go further into the two-body dynamics and investigate which launch conditions result in impact with Europa.

While impact with Jupiter can occur for non-elliptic trajectories, this is no more the case

for Europa. Indeed, in the event that the non-elliptic trajectory re-crosses the trajectory of Europa (after a fly-by of Jupiter), the time of travel between this crossing point and in the initial launch point is faster than the time Europa takes to reach that point along its orbit.

This condition on the energy imposes a strong constraint on the existence of impact with Europa (when launching from Europa), and in fact, restricts the existence of impact regions only for  $\theta$  close enough to  $2\pi/3$ , when  $C < C_{critical2}$ , as seen on Figure 12.

For  $E < 0$ , a sufficient condition for impact with Europa (in the two body setting) will occur if the elliptical orbit of the spacecraft intersects the circular orbit of Europa in the inertial frame. This will occur if the period of the spacecraft, given by

$$T = \frac{2\pi}{\sqrt{\mu}} \left( -\frac{1}{2E} \right)^{\frac{3}{2}} \quad (15)$$

is a multiple of a small fraction say  $n/m$  of Europa's period (i.e.,  $2\pi$  in our normalized setting), where  $m$  can be associated with the number of Europa revolutions around Jupiter and  $n$  with the number of spacecraft orbits (still around Jupiter). After  $m$  Europa orbits, the spacecraft will have made  $n$  orbits and will have returned to its original launch coordinates in space. Since Europa has also returned to its original position, impact will occur.

This condition is only a sufficient condition since along the trajectories shown in Figure 13, there are three additional points where impact with Europa could occur. However, these points are not considered here, since the first impact condition already yields a good picture of the strenght and weakness of the two body approximation.

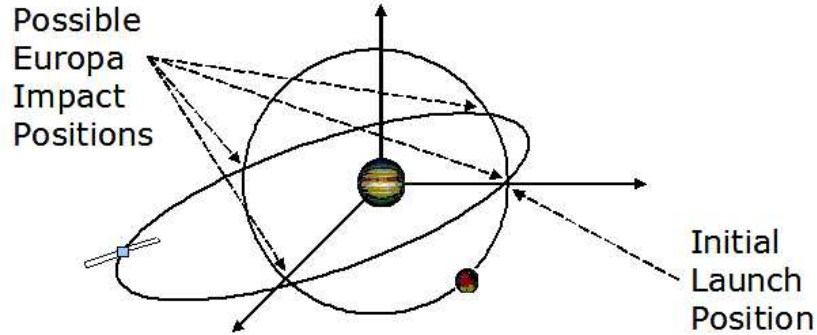


**Figure 13: Illustration of the four possible Europa impact locations in the two-body model.**

Re-expressing equation (15), using the sufficient condition above, we can see that impact occurs when the values of  $E$  satisfy the following relation:

$$E = -\frac{1}{2} \left( \frac{m}{n} \right)^{3/2} \quad (16)$$

This condition can be plotted for increasing value of the order of the fraction  $n/m$ , defined as  $n + m$  (the fraction being assumed to be in irreducible representation), which is

an indicator of the “strength” of the impact characteristic: lower orders correspond to quicker phenomena that are less susceptible to small perturbation. For example, the case  $n = m$  has order 2 (the smallest order physically meaningful) and corresponds to a spacecraft leaving Europa for one revolution around Jupiter before impacting with Europa again, the phenomena happening in a single Europa period. Figure 14 present the computation of the relation (16) as the order increases.

While these two body results for the Europa’s impact problem give us a basic understanding of these dynamics, the two body approximation in this setting is much more sensitive than for the Jupiter’s impact problem. For example, Figure 15 presents a comparison of the impact maps obtained using the two body and restricted three body models, respectively. As we can see, the nice one-dimensional two body problem dynamics are destroyed when perturbations are turned on. However, we can observe that the impact regions in the three body setting are still clustered along the main impact strip with Jupiter impact. It can also be observed that the density of these regions is larger where the density of impact lines with Europa at a given order in the two body approximation is larger.

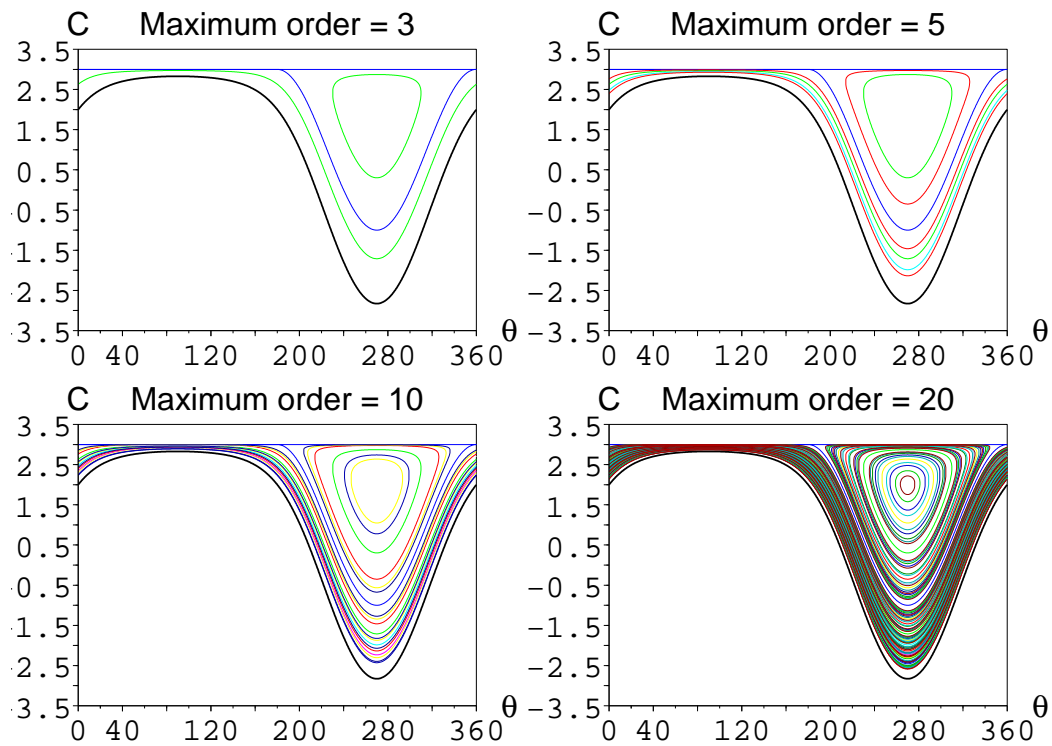


**Figure 14: Global view of the Europa impact dynamics for several orders in the planar case.**

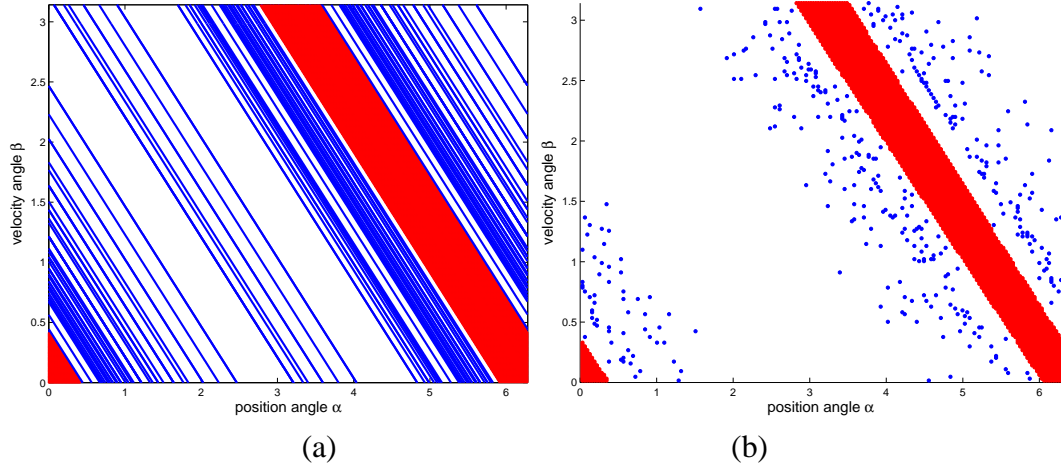


**Figure 15: Comparison between two body prediction and the computed impact maps for  $C=2.65$ : (a) two body solution; (b) three-body solution. (Red indicates impact with Jupiter and Blue indicates impact with Europa).**

## CONCLUSION

While the set of trajectories leaving the surface of Europa has its own intrinsic interest (as explained in the introduction), we should like to point out that the results reported here do also include some information on those trajectories that do not originate from Europa but do impact the moon when propagated forward in time.

Indeed, as can be readily observed from the equations of motion, the flow of the CR3BP is invariant under the transformation  $(x, y, z, \dot{x}, \dot{y}, \dot{z}, t) \rightarrow (x, -y, z, -\dot{x}, \dot{y}, -\dot{z}, -t)$ , which maps trajectories leaving the surface of Europa to trajectories impacting Europa. Given a point on a dynamical map, say  $(\alpha, \beta)$ , the application of the above symmetry results in changing the sign of  $\alpha$  and transforming  $\beta$  into  $2\pi - \beta$  (the velocity angle values now lie between  $\pi$  and  $2\pi$  in accordance with the impacting nature of the trajectory). Thus, by applying this transformation, the dynamical map generated for the trajectories leaving Europa now corresponds to a dynamical map of the trajectories impacting Europa, the map being generated over the impact location and velocity angle.

The case of a trajectory leaving Europa and impacting the moon after some number of revolutions (white dots in the maps presented in this article), is transformed into a trajectory with the same characteristics. However, the case of a trajectory leaving Europa and not impacting the moon for the given time span is transformed into a trajectory that do not originate from Europa but will impact the moon after a number of revolutions. These trajectories are most likely to represent the set of transfer trajectories that are sensitive to an eventual loss of thrust and should a priori be avoided. From the viewpoint of a landing probe, these transformed maps indicate for example the impact locations on Europa that a

non-controlled probe on a low energy trajectory would reach.

In the same realm of ideas, we note that the method presented here can in fact be extended to analyze a much larger class of motion by investigating the impact/non-impact dynamics of the set of trajectories leaving a sphere of arbitrary radius about Europa or Jupiter. Such a sphere would represent the set of possible transfers of all trajectories crossing that sphere. In particular, a low thrust transfer lying in an impacting region over a set of such consecutive spheres would represent a trajectory non-robust to an eventual loss of thrust.

Thus, a possible future direction would be to analyze the variation of the maps considered here with the two other parameters, kept fixed in this paper, that enter in their definition: the radius of the moon  $R_E$  and the mass parameter  $\mu$  that was used to model the Europa-Jupiter system. Finally, while the two body analysis presented in this paper applies to the spatial CR3BP, more numerical investigations of the spatial problem would be useful, as well as a deeper investigation of the transition between the low and high energy dynamical regimes.

## ACKNOWLEDGMENTS

This paper is the result of a summer project for students organized by IPAM and the authors would like to express their appreciation to the IPAM faculty and staff, especially Michael Raugh, Janice Amar, and Mark Green. It is also our pleasure to acknowledge the support from JPL as the industrial sponsor of this program. Finally, we would like to thank Prof. Alan Barr for letting us use the Barr Lab at Caltech and Marlys Murray and Louise Foucher of Caltech for taking care of some administrative matters.

## REFERENCES

1. Conley, C., "Low energy transit orbits in the restricted three-body problem", *SIAM Journal of Applied Mathematics*, Vol. 61, pp. 732-746, 1968.
2. Friedlander, A.L., "Jupiter Orbiter Lifetime - Hazard of Galilean Satellite Collision", *Journal of the Astronautical Sciences*, Vol. 23, No. 4, pp. 349-368, 1995.
3. Gomez, G., Koon W.S., Lo, M.W., Marsden, J.E., Masdemont, J., Ross, S.D., "Invariant Manifolds, the Spatial Three-Body Problem and Space Mission Design", Paper AAS 01-31, AIAA/AAS Astrodynamics Specialist Meeting, Quebec City, Canada, August 2001.
4. Howell, K., Barden, B., Lo, M., "Application of Dynamical Systems Theory to Trajectory Design for a Libration Point", *Journal of the Astronautical Sciences*, Vol. 45, No. 2, April-June 1997.
5. Lo M.W., et al., *Genesis Mission Design*, Paper No. 98-4468, AIAA/AAS Astrodynamics Conference, Boston, MA, August, 1998.

6. Lo, M.W., "Interplanetary Superhighway and The Origins Program", 2001, Web page: <http://www.gg.caltech.edu/mwl/publications/publications2.htm>.
7. McGehee, R., *Some Homoclinic Orbits for the Restricted Three-Body Problem*, Ph.D. thesis, University of Wisconsin, 1969.
8. Pollard, H., *Mathematical Introduction to Celestial Mechanics*, Prentice Hall, NJ, 1966.
9. Szebehely, V., *Theory of Orbits*, Academic Press, New York, 1967.
10. Villac, B.F., Scheeres, D.J., D'Amario, L.A., Guman, M.D., "The Effect of Tidal forces on orbit transfers", Paper AAS 01-247, 2001 AAS/AIAA Spaceflight Mechanics meeting, Santa Barbara, CA.
11. Villac, B.F., Scheeres, D.J., "New class of optimal plane change maneuvers", *Journal of Guidance, Control and Dynamics*, Vol. 26, No. 5, pp. 750-758, 2003.